Effects of combined dimension reduction and tabulation on the simulations of a turbulent premixed flame using a large-eddy simulation/probability density function method

Jeonglae Kim[a] & Stephen B. Pope[a]

[a] Sibley School of Mechanical and Aerospace Engineering, Cornell University, Ithaca, NY 14853, USA
Published online: 10 Jun 2014.

PLEASE SCROLL DOWN FOR ARTICLE

Taylor & Francis
Taylor & Francis Group

Effects of combined dimension reduction and tabulation on the simulations of a turbulent premixed flame using a large-eddy simulation/probability density function method

Jeonglae Kim* and Stephen B. Pope

Sibley School of Mechanical and Aerospace Engineering, Cornell University, Ithaca, NY 14853, USA

A turbulent lean-premixed propane–air flame stabilised by a triangular cylinder as a flame-holder is simulated to assess the accuracy and computational efficiency of combined dimension reduction and tabulation of chemistry. The computational condition matches the Volvo rig experiments. For the reactive simulation, the Lagrangian Large-Eddy Simulation/Probability Density Function (LES/PDF) formulation is used. A novel two-way coupling approach between LES and PDF is applied to obtain resolved density to reduce its statistical fluctuations. Composition mixing is evaluated by the modified Interaction-by-Exchange with the Mean (IEM) model. A baseline case uses In Situ Adaptive Tabulation (ISAT) to calculate chemical reactions efficiently. Its results demonstrate good agreement with the experimental measurements in turbulence statistics, temperature, and minor species mass fractions. For dimension reduction, 11 and 16 represented species are chosen and a variant of Rate Controlled Constrained Equilibrium (RCCE) is applied in conjunction with ISAT to each case. All the quantities in the comparison are indistinguishable from the baseline results using ISAT only. The combined use of RCCE/ISAT reduces the computational time for chemical reaction by more than 50%. However, for the current turbulent premixed flame, chemical reaction takes only a minor portion of the overall computational cost, in contrast to non-premixed flame simulations using LES/PDF, presumably due to the restricted manifold of purely premixed flame in the composition space. Instead, composition mixing is the major contributor to cost reduction since the mean-drift term, which is computationally expensive, is computed for the reduced representation. Overall, a reduction of more than 15% in the computational cost is obtained.

Keywords: LES/PDF simulation of turbulent premixed flame; RCCE; dimension reduction; ISAT; bluff-body stabilised flame

1. Introduction

1.1. *Lagrangian LES/PDF simulation of turbulent combustion*

Combustion models based upon a transported Probability Density Function (PDF) are very powerful for predicting turbulent combustion [1–3]. Compared to simple combustion models such as the laminar steady flamelet model [4], solving for the transport of a joint PDF has a distinct advantage in that it does not presume that chemical reactions are restricted to occur on a low-dimensional manifold [3]. Nonlinear chemical source terms appear in closed

---

*Corresponding author. Email: jeokim@stanford.edu.
Current address: Center for Turbulence Research, Building 500, Room 500A, 488 Escondido Mall, Stanford, CA 94305-3035, USA.

form, which is particularly important for predictions based upon Large-Eddy Simulation (LES), which should model the effects of unresolved scales where chemical reactions occur. As a result, strong turbulence–chemistry interactions such as local extinction and re-ignition can be studied with sufficient accuracy [5].

A prevalent approach for PDF combustion models is based upon the Lagrangian particle-mesh formulation [1], which approximates the transported PDF by the evolution of a large number of particles. High dimensionality of turbulent combustion is then efficiently handled. Coupled with LES, Lagrangian transported-PDF combustion models are promising in predicting realistic turbulent flames involving large unsteadiness and strong turbulence–chemistry interactions [2,3].

Recent efforts demonstrated that Lagrangian LES/PDF formulations are capable of predicting laboratory-scale turbulent flames with sufficient accuracy [6–14], mostly in non-premixed combustion regimes. However, their direct extension to turbulent premixed combustion should be done with some caution owing to fundamental differences in its physics compared to non-premixed flames [15]. Previous studies using PDF-based combustion models in a Reynolds Averaged Navier–Stokes (RANS) context have reported different modelling challenges, especially in composition mixing [16–19]. Also, premixed combustion demonstrates multiple regimes depending on turbulent scales [4,20], which become more complicated in an LES context where filter size is an important parameter [21].

1.2. *Chemistry calculation of transported-PDF combustion models*

One of the practical issues for the PDF-based prediction of turbulent combustion is its computational cost, as demonstrated by Hiremath *et al.* [11,22]. Directly incorporating detailed chemical mechanisms with many species and reaction steps often causes a serious increase in CPU time, which could make LES/PDF simulations intractable for realistic combustion of complex fuels. Thus, efficient calculation of chemistry is desired. In general, this can be practised by adopting mechanism reduction, dimension reduction and tabulation, as illustrated by Hiremath *et al.* [23]

In Situ Adaptive Tabulation (ISAT) is a very efficient tool for calculating chemical reaction [24]. For moderate-size chemical mechanisms (with up to $n_s = 50$ species, for example), the performance of ISAT is excellent and computational costs for reaction can be reduced, in general, by several orders of magnitude, compared to direct integration of Ordinary Differential Equations (ODEs). However, given large-size chemical mechanisms ($n_s = 100$ species, for example), direct application of ISAT may not guarantee good performance, owing to increased table size and search effort [23].

Dimension reduction is another strategy for the efficient computation of chemical kinetics. The basic idea is that a reduced set of variables is used to describe chemistry. Dimension reduction can be implemented in a number of different ways, such as by the Quasi Steady State Approximation (QSSA) [25,26], by the Invariant Constrained Equilibrium-edge Pre-Image Curve (ICE-PIC) [27] or by the Rate Controlled Constrained Equilibrium (RCCE) method [28,29]. For RCCE, instead of carrying full compositions, a reduced representation is judiciously selected and atoms from unrepresented species are carried as well for element conservation. Recently, Hiremath *et al.* [23] proposed a variant of RCCE. At each reaction step, the reduced representation is reconstructed so as approximately to recover the full compositions by using the Constrained EQuilibrium (CEQ) solver [30], followed by computing the reaction mapping. The last step is species reduction for the next reaction step. When coupled with ISAT, this procedure was demonstrated to be accurate

and efficient for Partially Stirred Reactor (PaSR) calculations [23] and for non-premixed jet flame simulations [11].

1.3. *Volvo validation experiment*

In the early 1990s, an extensive series of experiments was conducted at the Volvo facilities to validate an experimental rig for turbulent combustion [31,32]. The test section is a straight channel with a rectangular cross-section, and a bluff body placed across the channel serves to anchor the flame. The recirculation zone attached to the flame-holder provides the primary role of stabilising the premixed flame, increasing the residence time and continuously igniting fresh fuel–air mixture near the trailing edge. A series of experiments on the turbulent combustion of premixed propane–air mixtures at atmospheric pressure was conducted for a range of air mass-flow rates, equivalence ratios and unburnt mixture temperatures with two different types of flame-holder (V-gutter and stairs). These experimental conditions resulted in a wide range of turbulent premixed combustion regimes. Conventional LDA and gas analysis were performed to measure turbulence statistics, temperature and the species concentrations of combustion products [31]. In the follow-up study, non-intrusive two-wavelength Coherent Anti-Stokes Raman Scattering (CARS) was applied to provide space–time resolved flame characteristics and visualisation [32]. Owing to the relative scarcity of reliable and comprehensive experimental databases for turbulent premixed combustion [21], the quantitative thermo-chemical data sets of the Volvo experiment have been valuable for validating physical and numerical models for turbulent premixed combustion and for verifying the corresponding simulations [33–41].

1.4. *Objectives and challenges*

In this study, we apply combined dimension reduction and tabulation (RCCE/ISAT) to a bluff-body stabilised premixed flame, one of the turbulent premixed flames studied in the Volvo experiments [31,32]. The objective is to examine if RCCE/ISAT is accurate and efficient compared to ISAT alone in the framework of Lagrangian LES/PDF simulation in a similar way as did Hiremath *et al.* [11]. This involves efforts to apply the Lagrangian LES/PDF formulation to turbulent premixed combustion and assess its performance. A novel two-way coupling approach for density calculation [42] and modified Interaction-by-Exchange with the Mean (IEM) mixing model [43] are integrated. In addition to applying the Lagrangian LES/PDF formulation to a different combustion regime (premixed as opposed to non-premixed), combustion occurs at a fuel-lean condition very close to its lean blow-off limit, which gives additional complexity to turbulence–chemistry interaction. Also, the confined geometry and the reactive wake configuration cause strong unsteadiness. Unlike the piloted non-premixed jet flame of Hiremath *et al.* [11], the current premixed flame is stabilised by high-temperature combustion products within the recirculation zone formed behind a bluff body. The lack of hot pilot streams increases the sensitivity of the predicted flame to physical, kinetic and numerical models, especially near the flame-holder. Thus, only accurate prediction of the balance between molecular diffusion and reaction can result in a good comparison with the corresponding experimental measurements. All the aspects described above provide significant predictive challenges for LES/PDF simulations of the current turbulent premixed flame, which in turn establishes a good validation case for RCCE/ISAT versus ISAT alone for chemistry calculation.

2. Reactive simulation formulation

A turbulent premixed flame stabilised by a bluff-body flame-holder in the Volvo validation rig is predicted by LES/PDF simulation. The formulation is similar to those used by Wang and Pope [10] and Yang *et al.* [12]. The filtered conservation equations for mass, momentum and scalars are solved to obtain resolved velocity and scalar fields. Transported joint-PDF of composition is modelled by the evolution of a large number of notional particles. The particle positions and chemical compositions are obtained by solving stochastic differential equations. The two-way coupling between LES and PDF is achieved following Popov *et al.* [42] An additional transport equation for a scalar is time advanced with its solution approximating specific volume obtained as a result of chemical reaction, which provides an accurate and numerically stable density-coupling between LES and PDF. For efficient calculation of chemistry, ISAT is applied, within which the distribution of chemistry workload among participating cores and dimension reduction are performed by x2f_mpi [11] and RCCE, respectively.

2.1. *LES*

The filtered LES transport equations for mass, momentum and scalars are solved by the variable-density, low-Mach-number Navier–Stokes equation solver NGA [44], modified for two-way coupling of LES/PDF simulations. Variables are arranged in a staggered manner for discrete conservation of kinetic energy in the incompressible limit [45]. Solutions are time advanced by a second-order, semi-implicit, Crank–Nicolson scheme [46].

Resolved molecular viscosity $\tilde{\nu}$ and diffusivity $\tilde{\Gamma}$ are evaluated using an empirical power-law function of temperature [10] and equal diffusivity is assumed for every species (unity Lewis number).

$$\tilde{\nu} = \nu_0(\tilde{T}/T_0)^{n_\nu}, \tag{1}$$

$$\tilde{\Gamma} = c_0\nu_0(\tilde{T}/T_0)^{n_\Gamma}, \tag{2}$$

where $\nu_0 = 5.09 \times 10^{-5}\,\mathrm{m^2\,s^{-1}}$, $T_0 = 600\,\mathrm{K}$, $n_\nu = 1.7$, $c_0 = 1.24$ and $n_\Gamma = 1.74$.

For sub-grid-scale dissipation, the standard dynamic Smagorinsky model is applied [47,48]. The turbulent diffusivity is calculated assuming a constant turbulent Schmidt number,

$$\tilde{\Gamma}_T = \frac{\tilde{\nu}}{\mathrm{Sc}_T}, \tag{3}$$

where $\mathrm{Sc}_T = 0.4$, the same value as used inprevious LES/PDF simulations for turbulent premixed flames [14]. No sensitivity test is performed to examine the effects of turbulent Schmidt numbers.

A transport equation for a scalar modelling resolved specific volume is given by

$$\frac{\partial}{\partial t}(\bar{\rho}\hat{v}) + \frac{\partial}{\partial x_j}(\bar{\rho}\tilde{u}_j\hat{v}) = \frac{\partial}{\partial x_j}\left(\bar{\rho}\tilde{\Gamma}_T\frac{\partial\hat{v}}{\partial x_j}\right) + S_v + w_v, \tag{4}$$

where $\tilde{u}_j$ is the resolved velocity in the *j*th direction, S_v is the source term representing the rate of volume expansion due to molecular diffusion and reaction, and w_v is the

relaxation term

$$w_v = \bar{\rho}\frac{\tilde{v} - \hat{v}}{\tau}, \tag{5}$$

where $\tau = 4\Delta t$ in this study, following Popov *et al.* [42], and Δt is the computational time step size. The source term W_v is evaluated by particle composition evolution and averaged for LES cells [42]. The relaxation term s_v ensures consistency between the specific volume $\tilde{v}$ calculated from the PDF calculation and modelled specific volume $\hat{v}$ obtained by solving (4). Specific volume transport is computed using a third-order bounded QUICK scheme.

The mildly complex geometry for the V-shaped flame-holder is represented using the Immersed Boundary-Approximate Domain Method (IB-ADM) [49].

To couple with the PDF method, the LES provides resolved velocities, turbulent diffusivity and molecular diffusivities to the particles by interpolation.

2.2. *PDF method*

Given the resolved LES field, the transport of the one-point, one-time Eulerian PDF for chemical compositions is modelled by the evolution of a large number of notional particles. Each particle carries information on its location $X^*(t)$ and composition $\phi^*(t)$. The superscript * denotes a particle quantity or a quantity evaluated at the particle location by interpolation.

A constant pressure assumption for a low-Mach-number limit is made for reaction, and thus the thermo-chemical state is completely determined by the chemical composition $\phi = \{z, h_s\}$, where z contains specific moles of species and h_s is the mixture enthalpy. Thus, the length of ϕ is equal to $n_s + 1$, where n_s is the number of chemical species.

The particle positions and chemical compositions are governed by Langevin-type stochastic differential equations [43,50].

$$dX^*(t) = \left[\tilde{u} + \frac{1}{\bar{\rho}}\nabla(\bar{\rho}\tilde{\Gamma}_T)\right]^* + (2\tilde{\Gamma}_T^*)^{1/2}\,dW, \tag{6}$$

$$d\phi^*(t) = -\Omega_M^*(\phi^* - \tilde{\phi}^*)\,dt + \left[\frac{1}{\bar{\rho}}\nabla\cdot(\bar{\rho}\tilde{\Gamma}\nabla\tilde{\phi})\right]^*\,dt + S^*\,dt, \tag{7}$$

where W is an isotropic, vector-valued Wiener process, Ω_M is the scalar mixing frequency and S is the chemical source term. Following Yang *et al.* [12], the scalar mixing frequency is modelled by

$$\Omega_M = C_M\frac{\tilde{\Gamma} + \tilde{\Gamma}_T}{\Delta^2}, \tag{8}$$

where $C_M = 12$ and Δ is the LES filter width. In (6) and (7), the modified IEM model [43,50] is applied to model the conditional diffusion of the implied Eulerian PDF transport. This is done by introducing the mean-drift term explicitly computing molecular diffusion at particle locations and applying the modified Fick's law for a correct prediction of diffusive velocity, followed by applying the classical IEM model. One of the advantages is that it does not produce spurious sub-grid-scale scalar variance in the DNS limit [43,50]. Also, it supports a straightforward implementation of differential diffusion, which can be important

for turbulent premixed flames by altering a subtle balance between molecular diffusion and reaction.

To solve (6) and (7), a weakly second-order splitting algorithm [51] is applied and particle transport, mixing and reaction steps are sequentially evaluated. The solution procedure is integrated in the Highly-scalable PDF code (HPDF). A second-order predictor–corrector scheme [51] time advances (6) to obtain $X^*(t)$. To maintain the number of particles per cell approximately the same after their transport, a particle number control algorithm is applied at every time step. The nominal number of particles per cell is 20.

The change in chemical composition due to reaction is computed by ISAT. In massively parallel simulations of turbulent flames, it is known that some processors are involved in far more intense calculations of chemical kinetics than others. The immediate consequence is severe load imbalance causing substantial idle time and reducing the overall scalability of reactive flow simulations. For chemistry calculation using ISAT, some cores may have tables completely filled and thus direct evaluation of ODE is conducted, significantly reducing the efficiency of ISAT. An effective solution to this issue is to employ the Fortran parallel library x2f_mpi [11] performing vector-valued function evaluation. This was previously integrated and coupled with ISAT; extensive tests using PaSR [23] and a benchmark LES/PDF simulation for non-premixed jet flames [22] demonstrated that a strategy of partitioning cores and performing message passing therein significantly improved the load imbalance. This strategy, called Partitioned Uniform RANdom (PURAN) distribution [22], is applied to the current study.

The evolution of the particle positions and compositions provides density, temperature, species mass fractions, and source terms for the specific volume transport at the particle level. Cell means are then estimated using the cloud-in-cell approach and implicit smoothing operators are applied to reduce statistical fluctuations [43].

3. Simulation conditions

The simulation domain matches the test section of the Volvo rig shown in Figure 1 with the streamwise domain shortened by 30% both upstream and downstream to save computational cost. Simulations are conducted in Cartesian coordinates with x for the streamwise direction, y for the wall-normal direction, and z for the periodic spanwise direction. The origin is at the centre of the base surface of the flame-holder. The flame-holder is modelled by a V-shaped triangular cylinder. Its height is $h = 4$ cm and is used as a reference length scale. The domain size is $20h$, $3h$ and $3h$ in the streamwise, wall-normal and spanwise directions, respectively. The upstream and downstream lengths with respect to the flame-holder are $5h$ and $12h$, respectively. The channel blockage ratio induced by the flame-holder is 1/3. The LES transport equations are solved for the entire domain, while particles are distributed only for x greater than zero, assuming that flashback does not occur. Overall, 0.5 million cells are used with 157 and 101 points in the x- and y-directions, respectively. The grid is generated with non-uniform spacing such that cell-stretching ratios vary continuously. The

Figure 1.   A schematic diagram for the computational domain on the x–y plane. (Colour online.)

grid sizes are as follows: in the *x*-direction, 0.03*h* near the base surface, 0.28 at the outlet; and in the *y*-direction, 0.01*h* near the wall. The maximum grid stretching ratio is about 1.4. In the *z*-direction, 32 points are uniformly spaced with $\Delta z/h = 0.09$. The LES filter width is defined by $\Delta = (\Delta x \Delta y \Delta z)^{1/3}$. The grid resolution gives a total number of particles of 10 million (nominally).

At the domain inflow, a nearly uniform velocity profile is introduced with centreline velocity $U_{in} = 34\,\text{m}\,\text{s}^{-1}$. The inflow temperature is 600 K, corresponding to the heated propane–air mixtures in the Volvo experiment. This condition results in an inflow Mach number of 0.06, justifying the low-Mach-number assumptions invoked in the conservation equations and chemistry calculation.

At the PDF inflow ($x = 0$), particles enter the domain with their mass flux determined by the LES-resolved density and velocity fields and with their composition being that of the fresh mixture.

The fresh premixed propane–air is introduced at an equivalence ratio of $\phi = 0.6$. This is slightly higher than the lean blow-off limit [31] and corresponds to a condition where the experimentally-studied flame demonstrates strong unstable combustion characterised by large-scale reactive vortical structures similar to Karman vortex shedding [32].

The location of the particle inlet boundary is not varied to examine its effects on statistics. However, the assumption that reaction occurs only downstream of the flame-holder appears to be justified by previous studies of the same flame where no distinct flash-back event was reported (see for example [41]).

Convective conditions are applied at the outflow boundaries of both LES and PDF simulations. The particle compositions are initialised by setting their compositions to the fully-burnt composition obtained from a one-dimensional laminar premixed flame calculation by FlameMaster [52].

In high-speed flow experiments, even well-designed rigs often demonstrate a certain level of noise, which gives increased turbulence intensities at upstream regions where flow-induced unsteadiness does not exist. In the Volvo experiment matching with the current upstream condition, the upstream turbulence intensities are not negligible: 7% for the streamwise and 3% for the wall-normal directions. Non-negligible upstream turbulence intensities may cause earlier transition to turbulence and enhanced mixing downstream. Thus, the same turbulence intensity as in the experiment is imposed on the mean velocity profiles. The simple approach proposed by Klein *et al.* [53] is adopted to generate artificial inflow turbulence. Random numbers for each velocity component are generated and filtered so that they have approximately the desired turbulence statistics (such as velocity auto-correlation in this study). Homogeneous, isotropic conditions and the Taylor's hypothesis are invoked to generate artificial turbulent fluctuations for inflow data. A proposed improvement for artificial inflow turbulence by Kempf *et al.* [54] is implemented as well. Tests demonstrated that the current implementation generated consistent artificial turbulence similar to that of Klein *et al.* [53].

Two different propane mechanisms are investigated: a 30-species, 114-step skeletal mechanism and a 15-species, 44-step quasi-global reduced mechanism. The skeletal mechanism is a subset of the detailed propane mechanism [55] and the quasi-global model was modified for fuel-lean conditions [56]. Both propane mechanisms have previously been used to predict bluff-body stabilised flames [56]. FlameMaster is used to determine the properties of a freely-propagating laminar premixed flame predicted by each mechanism, for the same unburnt mixture properties as in the Volvo experiment. Some of the properties are shown in Table 1 and it should be noted that none of the flame thicknesses is well resolved by the current LES grid.

Table 1. A one-dimensional unstretched laminar premixed flame: $T_u = 600$ K for a fresh propane–air mixture; T_b for an adiabatic flame temperature; s_L for an unstretched laminar burning velocity; δ_L^0 for flame thickness based upon temperature difference and maximum gradient; δ_L for flame thickness based upon diffusion scales; and Γ_u for the molecular diffusivity of the unburnt mixture.

Mechanism	T_b (K)	s_L (cm s^{-1})	δ_L^0 (cm)[a]	δ_L (cm)[b]
30 species, 114 steps	1952.7	57.4	0.047	0.011
15 species, 44 steps	1944.0	53.2	0.048	0.009

[a]$\delta_L^0 = (T_b - T_u)/\max(|\partial T/\partial x|)$.
[b]$\delta_L = \Gamma_u/s_L$.

For time advancement, the time step size is $\Delta t = 4 \times 10^{-6}$ s, resulting in the maximum CFL number being approximately equal to 0.5. Two sub-iterations are made for each LES time step for better convergence.

The ISAT tabulation error tolerance is set to be $\varepsilon = 10^{-4}$ and the maximum memory for tabulation on each core is 600 MB. Two-dimensional tests confirmed that error tolerances smaller than 10^{-4} caused negligible changes. *A posteriori* tests demonstrated that none of the ISAT tables was completely filled up, confirming that 600 MB is sufficiently large.

The simulations are run primarily on TACC Lonestar and on NICS Kraken clusters using 120 cores. The LES domain is decomposed into 30 subdomains in the *x*-direction and four subdomains in the *y*-direction with each subdomain assigned to one core. The PDF domain is decomposed into six subdomains in the *x*-direction and 20 subdomains in the *y*-direction using an automatic domain decomposition algorithm based upon work-load estimation for each core. Based upon this, 20 cores are grouped into one partition within which the PURAN algorithm is performed for x2f_mpi calls.

4. Results

In this section, the results from a series of turbulent premixed flame simulations are examined. First, the baseline results obtained for the 30-species mechanism without RCCE (ISAT alone) are described, followed by the results from the 15-species mechanism with ISAT alone. Then, simulation results from RCCE coupled with ISAT are reported. RCCE is applied only to the 30-species mechanism since the 15-species mechanism is deemed sufficiently small in size that further dimension reduction may result in larger errors with only a modest cost reduction. However, the 15-species mechanism results with ISAT alone are compared with the RCCE/ISAT results with a comparable number of represented species. The computational performance of each case is comprehensively discussed.

All the simulations are time advanced until they reach a statistically-stationary state ($t \approx 0.2$ s). Then, statistics are collected and time averaged for approximately ten flow-through times, corresponding to 0.2 s. Statistics are also averaged in the periodic *z*-direction. The reported results are insensitive to either increasing the grid resolution by a factor of two in each direction (eight times more grid points) or doubling the nominal number of particles per cell.

4.1. *Baseline results with ISAT alone*

Figures 2(a) and 2(b) demonstrate instantaneous iso-surfaces of CO mass fraction and slices of temperature at several streamwise locations. The flame simulated using ISAT
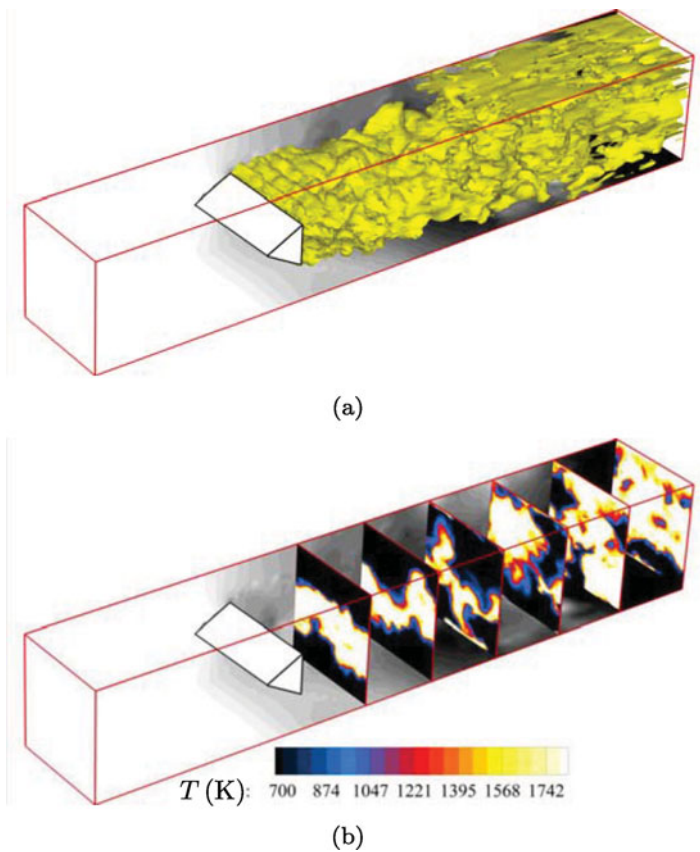
Figure 2.   (a) Instantaneous iso-surface of $Y_{CO} = 0.003$; (b) instantaneous contours of temperature at several streamwise locations. Both plots are obtained at $t = 0.2$ s. Grey-scale contours represent instantaneous pressure. (Colour online.)

alone and the 30-species mechanism is fully developed and stably attached to the flame-holder. The premixed flame sheet is initially two-dimensional near the separating edges of the flame-holder, but three-dimensionality quickly develops downstream. However, the asymmetry due to strong alternating large-scale structures is not as clearly visible as the observations of Fureby [34] and Ma *et al.* [41]

Figure 3 shows time-averaged streamwise velocity on the channel midplane ($y = 0$). The results from both the 30-species and the 15-species mechanisms are shown. For both cases, the mean recirculation length (defined by the streamwise location where mean velocity crosses $U = 0$ for $x > 0$) is shorter by h than the Volvo measurement; however, the rate at which the reactive wake recovers in the streamwise direction is predicted correctly. The wiggles for $x/h \gtrsim 3$ are caused by relatively poor spatial resolution and are not seen for simulations using a refined grid. Streamwise and wall-normal turbulence intensities on the midplane are shown in Figures 4(a) and 4(b), respectively. For $x/h \gtrsim 4$, the streamwise turbulence intensities significantly deviate from the experimental measurement for both mechanisms, while wall-normal turbulence intensities demonstrate mild differences. The large level of fluctuation for the Volvo measurement in Figure 4(a) is attributed to strong alternating large-scale structures; however, the maximum fluctuation at $x/h \approx 5$ is bigger
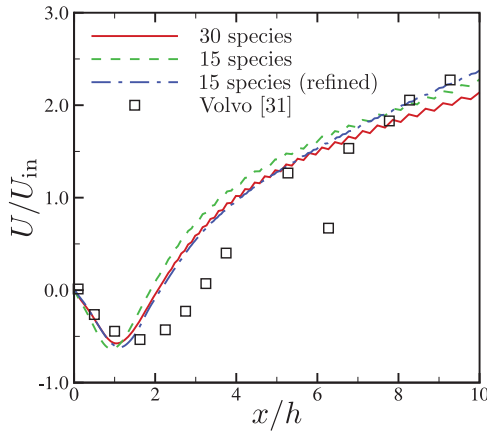
Figure 3.   Time-averaged streamwise velocity on the channel midplane ($y = 0$). (Colour online.)

than the local mean velocity, suggesting that the experimental data might include a certain amount of measurement error.

The profiles of time-averaged streamwise and wall-normal velocities are shown in Figures 5(a) and 5(b), respectively. Overall, the agreement is encouraging for both mechanisms. Some non-negligible discrepancies are observed especially for $x/h > 3.75$. As illustrated in Figure 5(b), the predicted flame demonstrates less asymmetry and the reactive wake recovers rather more quickly than the measurement for both mechanisms.

Figures 6(a) and 6(b) show the profiles of streamwise and wall-normal turbulence intensities. Again, the agreement is encouraging; however, the 15-species mechanism predicts somewhat higher levels of fluctuations for v'_{rms}, especially near the flame-holder. On the other hand, the 30-species mechanism shows a consistently good prediction except for $x/h = 9.4$. At $x/h = -5$, the inflow turbulence intensity is predicted correctly, verifying that the
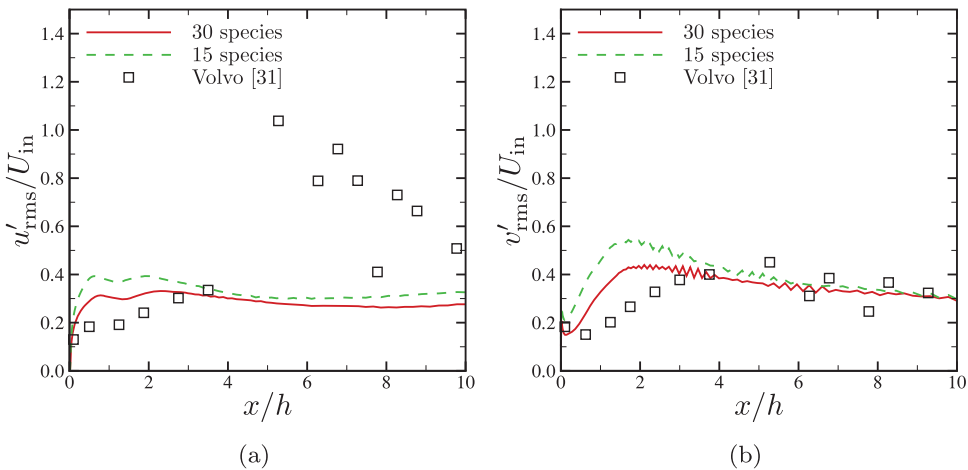

Figure 4.   (a) Streamwise and (b) transverse turbulence intensities on the channel midplane ($y = 0$). (Colour online.)
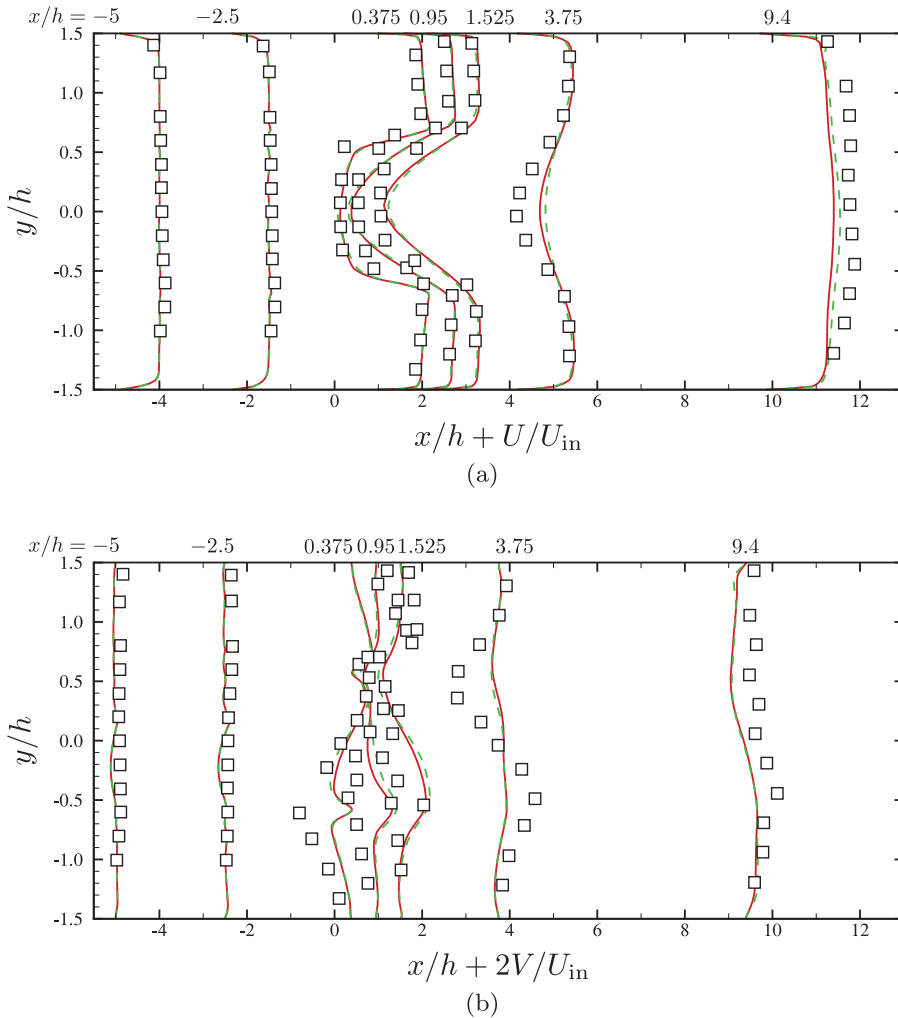
Figure 5.　(a) Mean streamwise and (b) mean transverse velocity profiles at several streamwise locations; solid line, 30 species; dashed line, 15 species; square symbol, the Volvo measurement [31]. (Colour online.)

filtering-based generation of artificial turbulence [53] reproduces the upstream condition of the corresponding experiment well.

　　Time-averaged temperature profiles are compared in Figures 7(a) and 7(b) at two streamwise locations. The 15-species mechanism underpredicts the maximum temperature at $x/h = 3.75$. However, its agreement at $x/h = 8.75$ is slightly better than the 30-species mechanism result.

　　Also shown on Figures 7(a) and 77(b) are the CARS measurements data [32]. As pointed out by Sjunnesson *et al.* [32], there are substantial differences between the two experimental measurements and the true temperature would lie somewhere between the two curves.

　　For both cases, there are high-temperature pockets near the upper channel wall. Their existence is qualitatively evidenced by Figure 2(a) for a higher concentration of CO near the upper wall. Thus, asymmetry is introduced to the profiles at $x/h = 8.75$. Presumably,
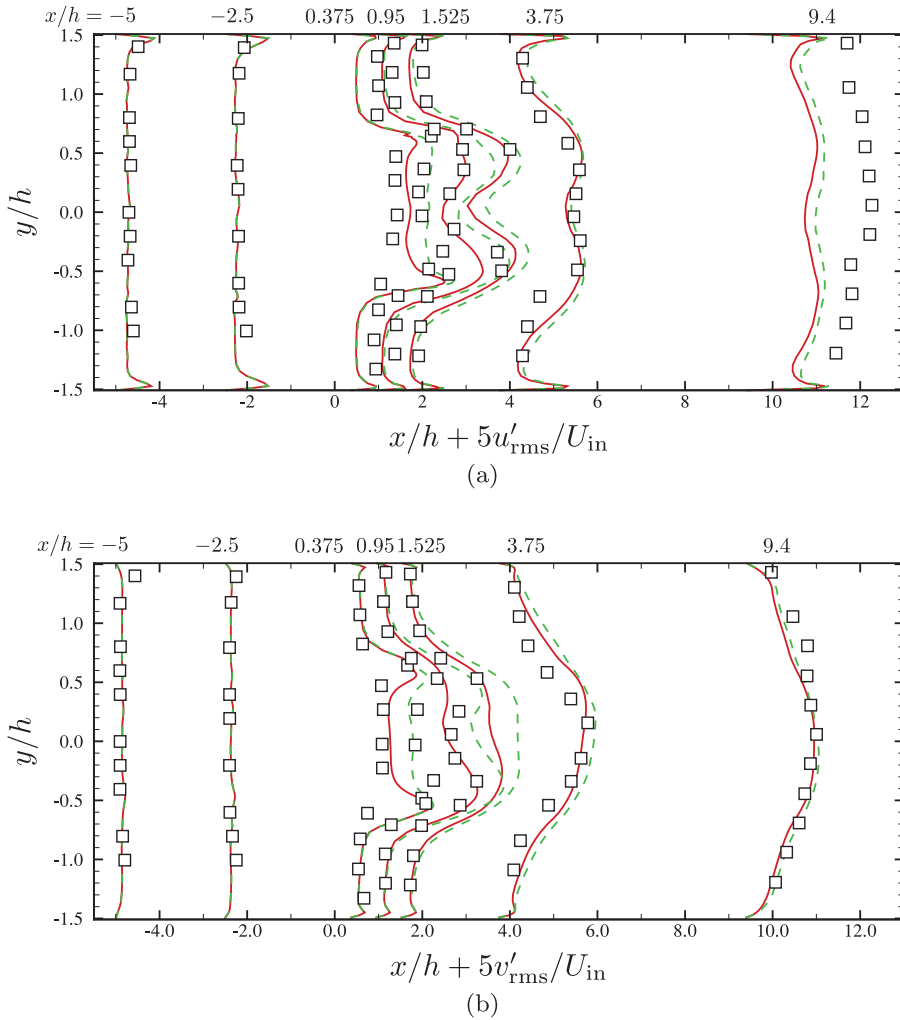
Figure 6. (a) Streamwise and (b) transverse turbulence intensities at several streamwise locations; solid line, 30 species; dashed line, 15 species; square symbol, the Volvo measurement [31]. (Colour online.)

fresh fuel–air mixture near the upper channel wall is ignited by strong unsteadiness of the flame structures downstream and stabilised near the wall. Pockets of burning regions persist for a long time, presumably due to low velocities near the wall, and this affects the temperature statistics. Note that in the current LES/PDF formulation where solid walls are modelled adiabatically, no account is taken of the quenching effect of the wall, while the top and bottom channel walls in the Volvo rig are water cooled. The geometry, governing equations and initial and boundary conditions do not introduce any asymmetry about the channel midplane $y = 0$. The observed asymmetry in the solution appears stable in time and occurs on either side of the midplane for different realisations of the flame.

Similar observations can be made for the time-averaged mass fraction of CO in Figures 8(a) and 8(b). At $x/h = 3.75$, the peak magnitudes of CO are predicted well
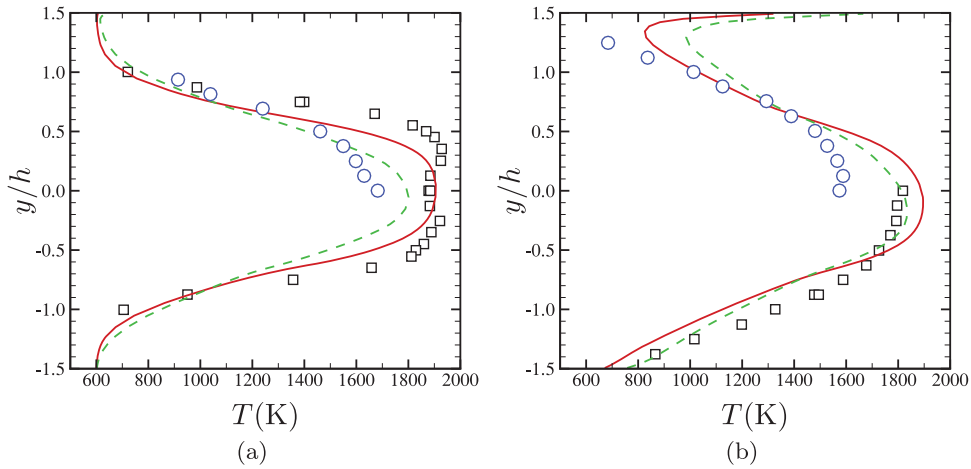
Figure 7. Time-averaged temperature at (a) $x/h = 3.75$ and (b) 8.75; solid line, 30 species; dashed line, 15 species; rectangle symbol, gas analysis [31]; circle, CARS measurements [32]. (Colour online.)

by the 30-species mechanism, while the 15-species mechanism calculation shows significantly lower peak levels of CO, consistent with its smaller maximum temperature than the experiment in Figure 7(a). Within the recirculation zone ($-0.5 < y/h < 0.5$), CO mass fractions are consistently higher than measurement for both mechanisms. Using a larger-size, more complex propane mechanism (30 species as opposed to 15 species) reduces the discrepancy. It is also likely that the higher laminar burning velocity of the 30-species mechanism (see Table 1) may contribute to the better agreement; however, this was not analysed further.

Another important observation is the rather large value of C_M compared to the standard choice of $C_M = 4$, which yields very poor agreement with the experimental measurements,
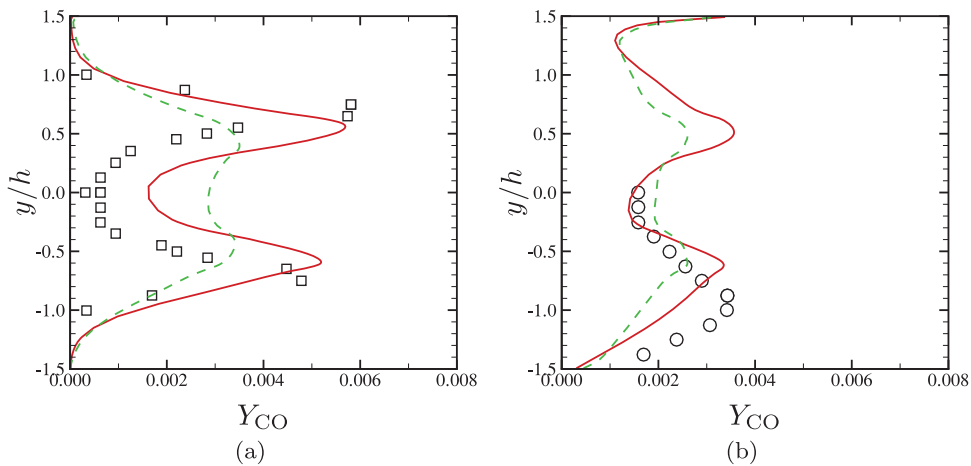

Figure 8. Time-averaged mass fractions of CO at (a) $x/h = 3.75$ and (b) 8.75; solid line, 30 species; dashed line, 15 species; symbol, the Volvo measurement [31]. (Colour online.)
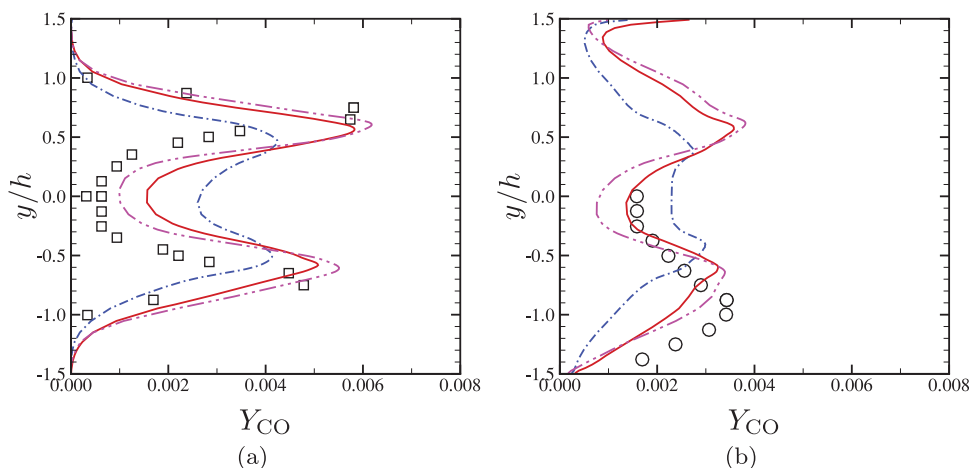
Figure 9. Time-averaged mass fractions of CO at (a) $x/h = 3.75$ and (b) 8.75; solid line, $C_M = 12$; dashed-dot line, $C_M = 4$; dashed-dot-dot line, $C_M = 16$; symbol, the Volvo measurement [31]. The results are obtained using the 30-species mechanism. (Colour online.)

as can be seen in Figures 9(a) and 9(b). This was also reported previously for turbulent premixed flame simulations [14,18] where transported PDF combustion models and a similar value of the scalar mixing frequency coefficient (i.e. $C_M = 8$) were used. Thus, C_M is systematically varied to find out whether calculations using the value $C_M = 12$ reasonably match the Volvo measurement data.

At $x/h = 3.75$, increasing C_M (greater than the default value of 12) significantly improves the agreement, suggesting that the actual reaction is more rapid and localised at the premixed flame front; however, the agreement at $x/h = 8.75$ becomes worse for a larger value of C_M (see Figure 9(b)), presumably due to the scalar mixing made artificially faster by increasing C_M. This is justified by an observation that reaction near the flame-holder is more likely governed by fast laminar flamelet-like combustion with higher Damköhler numbers, while turbulence–chemistry interactions downstream shift the regime to the wrinkled or corrugated flamelet regime [41]. Thus, a higher value of C_M predicts the near-field flame characteristics better, while a smaller value is better suited downstream. This also implies that using a single, constant value of C_M does not predict the correct balance between molecular diffusion and reaction for the current turbulent premixed flame. Similar observations have been made before and several models have been proposed for turbulent premixed flames to address the issues in the LES/PDF context [57] and in the RANS/PDF context [16–19]. This could also be attributed to the limitation of the current scalar mixing frequency model (8) given as a function of the effective diffusivity and a local filter size.

Since the objective of the current study is to assess the accuracy and efficiency of RCCE/ISAT versus ISAT alone for a reasonably good LES/PDF simulation, no further analysis was made, which is, however, certainly very interesting to study.

Overall, the LES/PDF simulations of the baseline cases using ISAT alone demonstrate reasonably good agreements with the Volvo rig measurements for the two different propane mechanisms. Those mechanisms result in significantly different calculations of the same species (e.g. CO), and in general the 30-species mechanism yields better agreement with the experimental data. In the next section, comparisons with RCCE/ISAT in the same configuration are provided for the 30-species propane mechanism.

4.2. *Choosing 'good' represented species*

The performance of RCCE/ISAT can be affected by the choice of represented species and it is always useful to select 'good' represented species. In general, fuel, oxidiser and major product species are chosen along with other minor species to be compared with the corresponding measurements. A quick and intuitive solution is to examine the relative magnitudes of each species mass fraction in a one-dimensional flame profile and select species having non-negligible mass fractions. A more elaborate approach is to apply systematic algorithms minimising a measure of dimensional reduction errors. In this study, we take both approaches to select 'good' represented species. For the latter approach, a PaSR with the Greedy algorithm [58] and a PaSR with the Greedy Algorithm with Local Improvement (GALI) [23] were examined. GALI is based upon the Greedy algorithm and systematically finds approximately optimal sets of species minimising dimensional reduction errors compared to the corresponding full-composition calculation. In this study, the simpler PaSR is used to avoid prohibitive computational cost when either the Greedy or GALI algorithm is directly applied to LES/PDF.

RCCE is applied only to the 30-species skeletal mechanism. Since elements in unrepresented species are also carried by the particles (for element conservation), C, H, O, Ar and N atoms are also included in the reduced representation. Since there are five additional variables for the elements, the maximum number of represented species is limited to 25 (if applying RCCE is intended for a cost reduction).

Two sets of represented species are examined: $n_{rs} = 11$ and 16 represented species. Thus, the reduced representations contain 16 and 21 variables, respectively. Both the Greedy algorithm and GALI return sets consisting of a reduced number of species, approximately minimising the dimension reduction error illustrated in Figure 10. However, for 11 represented species, the CEQ solver called by RCCE fails (the Greedy algorithm and GALI demonstrate the same error for 11 represented species). Thus, a one-dimensional laminar flame profile is instead used to pick 11 species in descending order of mass fractions.

For the 16 represented species, GALI identifies a set of species with a smaller error than the Greedy algorithm; however, the resulting reduced representation does not include
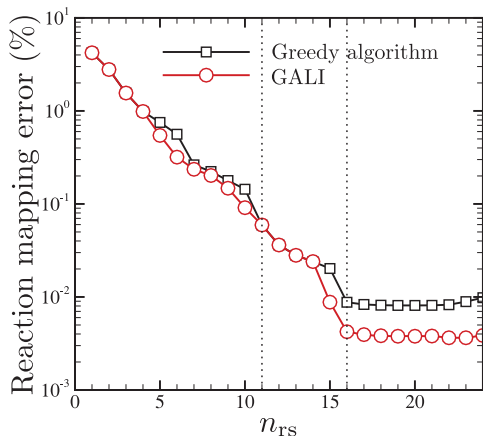

Figure 10. Relative reaction mapping error with respect to the number of represented species n_{rs} for the 30-species mechanism. (Colour online.)
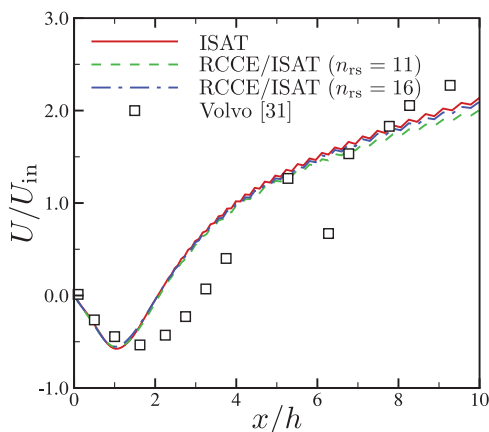
Figure 11.   Time-averaged streamwise velocity on the channel midplane ($y = 0$). (Colour online.)

CO, an important species compared with the Volvo rig measurement. Thus, the result from the Greedy algorithm containing CO is selected for the 16 represented species.

The represented species for both cases are listed in Table 2.

4.3.   *RCCE/ISAT versus ISAT: Computational accuracy*

For the turbulent premixed flames discussed in the last section, the dimension-reduction algorithm RCCE is applied in conjunction with ISAT to examine its computational accuracy and efficiency. As mentioned earlier, only the 30-species mechanism is investigated. The same as ISAT alone, simulations using RCCE/ISAT are time advanced for ten flow-through times and statistics are collected and analysed for another ten flow-through times.

Figures 11, 12, 13 and 14 show turbulence statistics similarly to those presented in Section 4.1. Also shown are the results from RCCE/ISAT simulations for the two different sets of represented species ($n_{rs} = 11$ and 16; see Table 2). For every comparison made, the differences in turbulence statistics between RCCE/ISAT and ISAT alone are negligible.

Figures 15 and 16 show comparisons for temperature and CO mass fraction between RCCE/ISAT and ISAT. Similar to the turbulence statistics, three calculations are essentially indistinguishable. Therefore, RCCE/ISAT runs for two different reduced representations predict the current turbulent premixed flame as accurately as the run with ISAT alone.

Table 2.   'Good' represented species selected from the 30-species mechanism: 11 represented species chosen based upon the mass fractions of a one-dimensional laminar flame and 16 represented species using the Greedy algorithm.

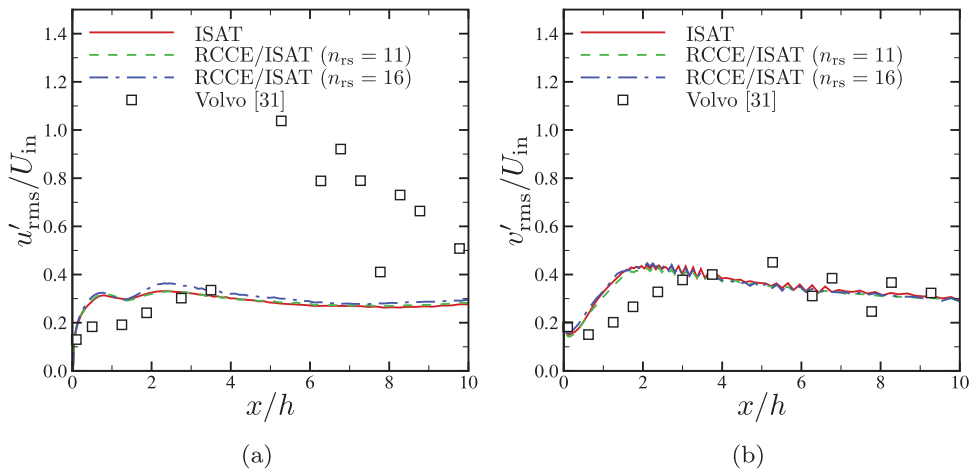| Number of represented species (n_{rs})	Represented species
11	C_3H_8, CO_2, C_2H_4, H_2, O_2, O, OH, CO, HO_2, H_2O, H
16	C_3H_8, CO_2, C_2H_4, C_3H_6, H_2, O_2, CH_4, C_2H_2, O, CH_2O, OH, CO, H_2O_2, C_2H_6, HO_2, H_2O

Figure 12.   (a) Streamwise and (b) transverse turbulence intensities on the channel midplane ($y = 0$). (Colour online.)

4.4.   *RCCE/ISAT versus ISAT: Computational efficiency*

In the last section, the solutions obtained from LES/PDF simulations using RCCE/ISAT are compared with those using ISAT alone. It is concluded that RCCE/ISAT provides as accurate predictions as ISAT alone for turbulence and flame statistics. Since particles carry a reduced representation of the full compositions, previous studies found that a significant reduction in computational cost can be obtained [11,23]. In this section, the simulation results are analysed to quantify how much cost reduction is possible for the current configuration.

4.4.1.   *Timing statistics with ISAT alone*

Before discussing the performance of RCCE/ISAT, the timing statistics of LES/PDF simulations without dimension reduction (ISAT alone) are discussed for the 30-species propane mechanism. For the statistically-stationary turbulent premixed flame simulation obtained in Section 4.1, an LES/PDF simulation using ISAT alone is run for 5000 time steps, corresponding to one flow-through time. The ISAT tables are initially empty. As shown in Table 3, approximately 90% of wall-clock time is spent for evolution of particle positions and compositions. Interestingly, most of the wall-clock time is used for particle transport and mixing (including the mean-drift term in Equation 7). This is quite different from the wall-clock time statistics obtained for a turbulent non-premixed jet flame using a 38-species methane–air mechanism [11], where chemistry took more than 80% of wall-clock time in the LES/PDF simulation (with PLP strategy). Even accounting for the current modified IEM model being more expensive (twice, at most) than the classical IEM model used in Hiremath *et al.* [11], this reduction in the relative computational cost for the reaction step is huge. As shown in Table 3, reaction is less expensive than solving the LES transport equations, estimating moments for LES cells and interpolating LES-resolved fields to each particle. Note that Hiremath *et al.* [11] computed transport and mixing only once ($\mathbb{TMR}$ operator splitting), but they kept the nominal number of particles per PDF cell twice as large ($n_{pc} = 40$) as in the current study ($n_{pc} = 20$). Thus, their transport and mixing steps were likely to be as costly as the current ones using $\mathbb{TMRMT}$ operator splitting, where transport and mixing steps are evaluated twice. The current ISAT error tolerance $\varepsilon = 10^{-4}$
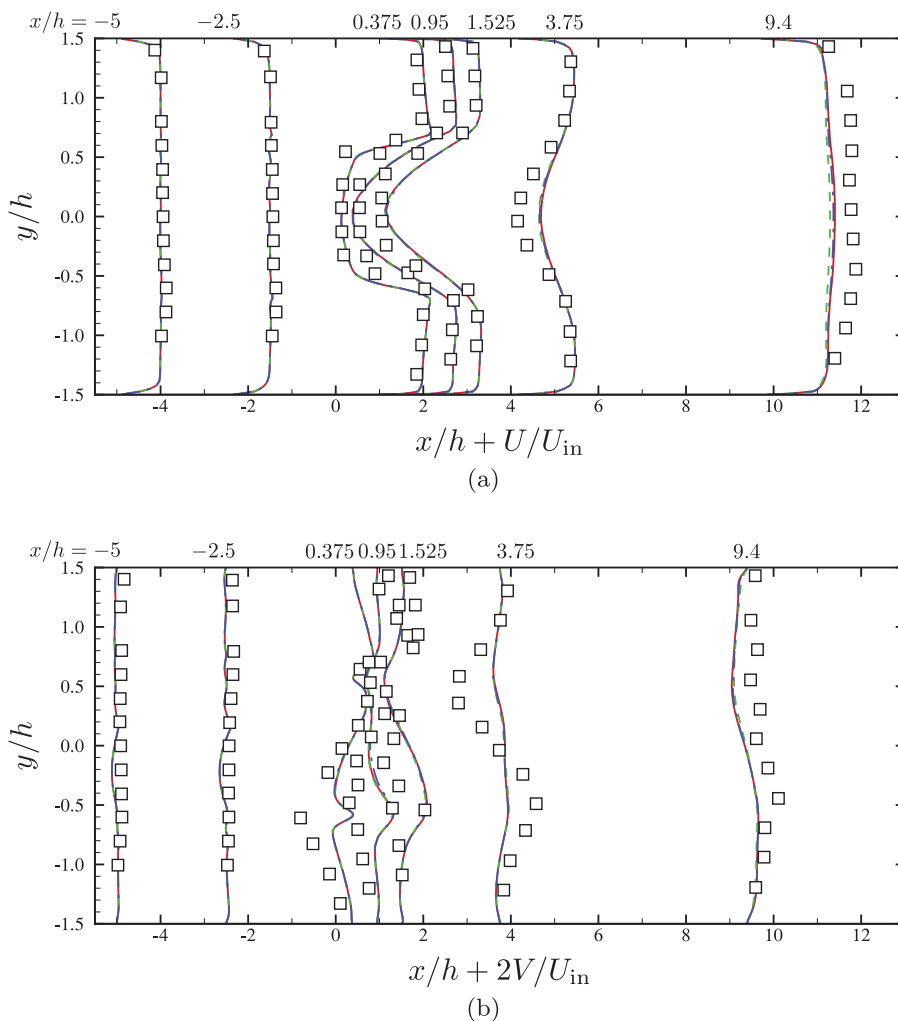
Figure 13. (a) Mean streamwise and (b) mean transverse velocity profiles at several streamwise locations; solid line, ISAT; dashed line, RCCE/ISAT ($n_{rs} = 11$); dashed-dot line, RCCE/ISAT ($n_{rs} = 16$); symbol, the Volvo measurement [31]. (Colour online.)

is the same as Hiremath *et al.* [11] and the maximum storage assigned to the ISAT table per core is 60% of their 1000 MB per core.

This substantial reduction in computational cost for the reaction step is attributed to the purely premixed flame configuration. A purely premixed flame can be tabulated very efficiently for its relatively simple manifold structure in composition space, whereas non-premixed combustion requires additional parameterisation based upon mixture fraction. As a result, none of the current ISAT tables is completely filled up at any core for this 5000-step test run. At the last time step, only 6% of the maximum table entries are filled up, while some tables were reported to be completely filled in Hiremath *et al.* [11]. Note that Hiremath *et al.* [11] time integrated for 2000 time steps (5000 steps for the current study) and 1.7 times more memory was assigned to ISAT table per core. Also, it takes only 80 s to build ISAT tables (approximately 10% of overall reaction time), compared to the hour-long
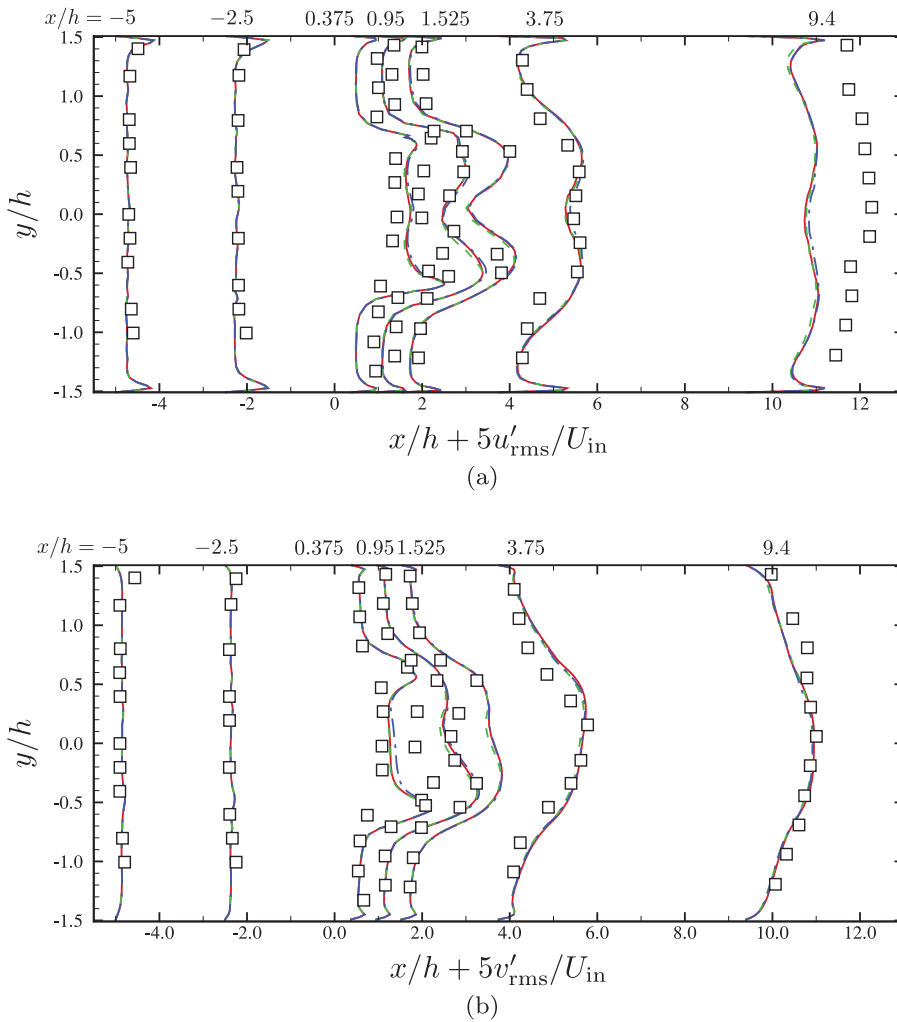
Figure 14.   (a) Streamwise and (b) transverse turbulence intensities at several streamwise locations; solid line, ISAT; dashed line, RCCE/ISAT ($n_{rs} = 11$); dashed-dot line, RCCE/ISAT ($n_{rs} = 16$); symbol, the Volvo measurement [31]. (Colour online.)

build-time of Hiremath *et al.* [11]. The table build-time is defined in the same way as in Hiremath *et al.* [23] (total tabulation time minus retrieval time). Almost every query is resolved by the primary retrieval with zero direct evaluation. These observations support the restricted manifold structure of the current turbulent premixed flame in the composition space and additionally demonstrate the efficiency of the ISAT approach. More quantitative comparison for ISAT statistics follow below.

4.4.2.   *x2f_mpi performance*

The timing statistics in Table 3 implies that reaction is not a major contributing factor to the overall computational cost of the current LES/PDF simulation for a turbulent premixed flame. Then, it follows that x2f_mpi strategies designed to resolve severe load imbalance
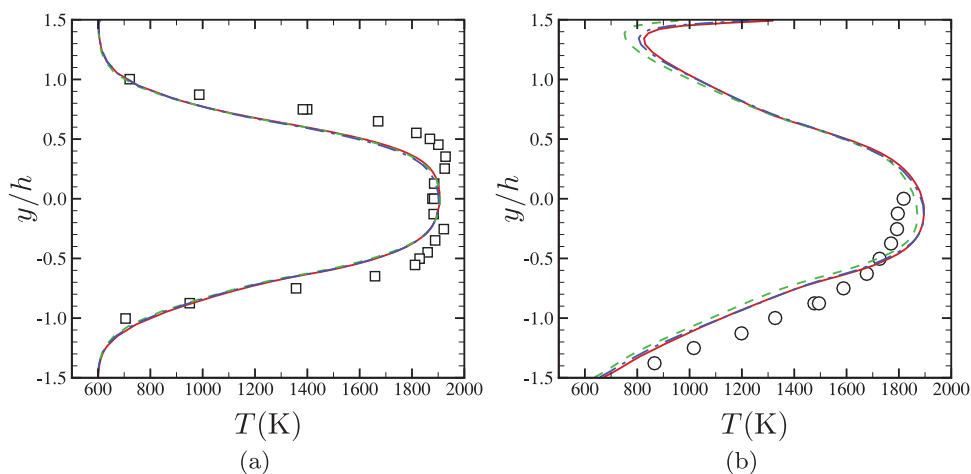
Figure 15. Time-averaged temperature at (a) $x/h = 3.75$ and (b) 8.75; solid line, ISAT; dashed line, RCCE/ISAT ($n_{rs} = 11$); dashed-dot line, RCCE/ISAT ($n_{rs} = 16$); symbol, the Volvo measurement [31]. (Colour online.)

incurred by chemistry calculation is not likely to result in much speed-up as reported in Hiremath *et al.* [22]. This is tested and confirmed; among available x2f_mpi strategies, PLP, URAN and PURAN, none of them is able to gain any significant speed-up observed previously for a turbulent non-premixed jet flame [22]. The URAN strategy, by design, increases the computational cost slightly compared to PLP for its additional message passing over the entire cores. PURAN works out to be as expensive as PLP for its modest increase in message passing.
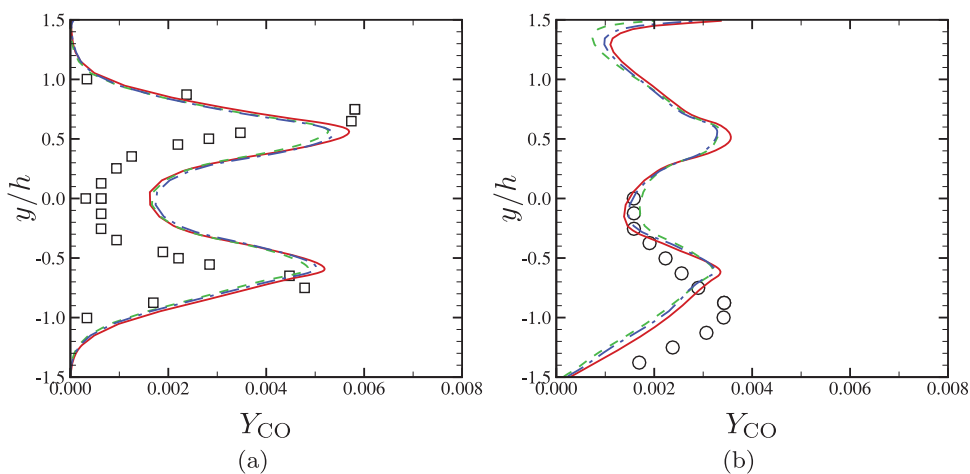

Figure 16. Time-averaged mass fractions of CO at (a) $x/h = 3.75$ and (b) 8.75; solid line, ISAT; dashed line, RCCE/ISAT ($n_{rs} = 11$); dashed-dot line, RCCE/ISAT ($n_{rs} = 16$); symbol, the Volvo measurement [31]. (Colour online.)

Table 3. Relative wall-clock times for each module in LES/PDF simulation.

Modules	Wall-clock time with respect to LES/PDF (%)	Wall-clock time with respect to PDF (%)
LES	10	11
PDF[a]	90	100
Moment estimation and interpolation	13	14
Transport, mixing, reaction, and others	77	86
Transport	28	31
Mixing	33	37
Reaction	7	8
Others[b]	9	10

[a]Transport, mixing, reaction and others plus moment estimation and interpolation.
[b]Particle number control, particle boundary condition, particle check-pointing and two-way coupling source terms.

4.4.3. *Cost comparison between RCCE/ISAT and ISAT*

Figure 17 shows a comprehensive overview of timing statistics in the wall-clock time. The simulation result using ISAT alone for the 15-species reduced mechanism is plotted together for comparison. Overall, the computational cost is largest for the baseline case with ISAT alone (30 species). The wall times for RCCE/ISAT ($n_{rs} = 11$) and ISAT (15 species) are comparable to each other. This is because the reduced representation consists of the 11 represented species plus 5 elements for unrepresented species. Thus, the total number of
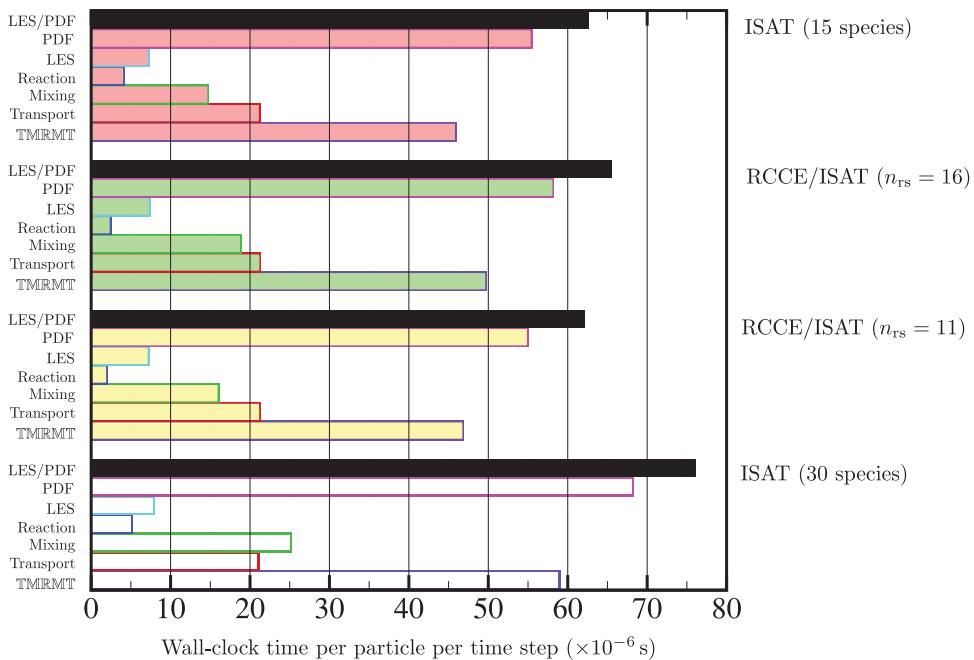

Figure 17. Wall-clock time statistics for the computational modules of the current LES/PDF simulations. $\mathbb{TMRMT}$ represents wall-clock time for particle transport, mixing, reaction, mixing, and particle transport. (Colour online.)

Table 4. Comparisons of wall-clock times per particle per time step for the mixing and reaction steps. The reductions are measured relative to the 30-species propane skeletal mechanism with the full composition.

Number of represented species (n_{rs})	Mixing			Reaction		
	Wall time (μs)	Reduction (μs)	Reduction (%)	Wall time (μs)	Reduction (μs)	Reduction (%)
11/30 (RCCE/ISAT)	16.00	9.14	36	1.98	3.18	62
16/30 (RCCE/ISAT)	18.84	6.30	25	2.43	2.73	53
30 (full composition)	25.14	0	0	5.16	0	0
15 (full composition)	14.73	10.41	41	4.12	1.04	20

variables in the chemical compositions carried by the particles is almost the same, which can be seen from comparable wall times between two cases on the mixing step. Wall times for particle transport and LES are not affected by RCCE, as expected. Overall reductions in the computational cost are 15% for $n_{rs} = 11$ and 18% for $n_{rs} = 16$.

As can be seen in Table 4, the application of RCCE in conjunction with ISAT achieves its dominant reduction in computational cost on the mixing step: 36% reduction for RCCE/ISAT (11/30 species) and 25% reduction for RCCE/ISAT (16/30 species). Considering that the classical IEM model implementation contributes only a fraction of computational cost, the reduction appears to come from evaluating the mean-drift term in the particle composition equations (7). For the reaction step, a 62% reduction is obtained for RCCE/ISAT (11/30 species) and a 53% reduction for RCCE/ISAT (16/30 species). Although the relative reductions are much larger for the reaction step, their contribution to the overall cost reduction is less than half of the mixing step.

5. Conclusions

The computational efficiency and numerical accuracy of RCCE coupled with ISAT are assessed for a bluff-body-stabilised confined flame using the transported-PDF turbulent combustion model. The inherent unsteadiness of turbulent lean-premixed flames in the confined combustor configuration makes LES particularly suitable. The novel LES/PDF two-way coupling and the modified IEM model with mean drift are integrated and used. An immersed boundary method is applied to simulate the flow around the flame-holder. For efficient load distribution for chemistry calculation, the PURAN algorithm using the x2f_mpi library is applied. Two propane mechanisms developed by CSE are tested: a 30-species, 114-step skeletal mechanism, and a 15-species, 44-step reduced mechanism.

The simulation results demonstrate reasonably good agreement with the corresponding experimental measurements for turbulence statistics, mean temperature, and species mass fractions. Purely premixed combustion produces a restricted manifold in the composition space which can be tabulated very efficiently by ISAT. A consequence is that ISAT table sizes are significantly smaller than in non-premixed flame calculations and reaction takes only a minor portion (less than 10%) for overall computational loads. Thus, PLP, URAN and PURAN strategies in x2f_mpi do not achieve any improvement in CPU time.

The baseline case with ISAT alone is established using the 30-species skeletal mechanism. From this 30-species mechanism, the 11 and 16 represented species are chosen based upon a one-dimensional laminar premixed flame profile and PaSR calculations with the Greedy algorithm. GALI is also applied to select good represented species; however,

the reduced representation found by GALI does not include important quantities to compare with the experiment and thus its result is not used. The RCCE/ISAT results demonstrate excellent agreement for every quantity examined, compared to the baseline case with ISAT alone.

The reduction in the computational cost is most significant for the fractional mixing step (36 and 25% reductions for 11 and 16 represented species, respectively), since only the reduced representation of compositions is carried by the particles. The saving mainly comes from evaluating the mean-drift terms, modelling the conditional diffusion. The cost reduction for the reaction step is somewhat modest since reaction does not dominate the CPU time for the current purely premixed combustion calculation. However, their magnitudes of relative reductions compared to the full-composition ISAT result are 62 and 53% for the 11 and 16 represented species, respectively.

While the cost reduction is not particularly large, the current study unambiguously demonstrates that there is a clear reduction in computational cost even in a purely premixed combustion regime where chemistry calculation takes almost a negligible portion and thus, the combined dimension reduction and tabulation may not obtain its best performance. Also, the conclusion of the current study suggests that more resolved simulations with a larger number of particles or with a chemical mechanism of many species can benefit more substantially from the combined dimension reduction and tabulation. Also, it is expected that the current RCCE/ISAT approach can be more effective for partially premixed flames where the composition manifold structures are more complicated.

The present study successfully demonstrates that the combined dimension reduction and tabulation RCCE/ISAT is both accurate and efficient for computing turbulent premixed flames exhibiting unstable combustion at a fuel-lean condition. Our results verify the previous findings about the accuracy and efficiency of RCCE/ISAT [11,23] and extend its applicability to turbulent premixed flame configurations with mildly complex geometry.

References

[1] S.B. Pope, *PDF methods for turbulent reactive flows*, Prog. Energy Combust. Sci. 11 (1985), pp. 119–192.
[2] D.C. Haworth, *Progress in probability density function methods for turbulent reacting flows*, Prog. Energy Combust. Sci. 36 (2010), pp. 168–259.

[3] S.B. Pope, *Small scales, many species and the manifold challenges of turbulent combustion*, Proc. Combust. Inst. 34 (2013), pp. 1–31.

[4] N. Peters, *Turbulent Combustion*, Cambridge University Press, Cambridge, UK, 2000.

[5] R. Cao and S.B. Pope, *The influence of chemical mechanisms on PDF calculations of non-premixed piloted jet flames*, Combust. Flame 143 (2005), pp. 450–470.

[6] M.R.H. Sheikhi, T.G. Drozda, P. Givi, F.A. Jaberi, and S.B. Pope, *Large eddy simulation of a turbulent nonpremixed piloted methane jet flame (Sandia Flame D)*, Proc. Combust. Inst. 30 (2005), pp. 549–556.

[7] V. Raman and H. Pitsch, *A consistent LES/filtered-density function formulation for the simulation of turbulent flames with detailed chemistry*, Proc. Combust. Inst. 31 (2007), pp. 1711–1719.

[8] M.R.H. Sheikhi, P. Givi, and S.B. Pope, *Frequency-velocity-scalar filtered mass density function for large eddy simulation of turbulent flows*, Phys. Fluids 21 (2009), Paper No. 075102. Available at http://dx.doi.org/10.1063/1.3153907.

[9] M.B. Nik, S.L. Yilmaz, P. Givi, M.R.H. Sheikhi, and S.B. Pope, *Simulation of Sandia Flame D using velocity-scalar filtered density function*, AIAA J. 48 (2010), pp. 1513–1522.

[10] H. Wang and S.B. Pope, *Large eddy simulation/probability density function modeling of a turbulent $CH_4/H_2/N_2$ jet flame*, Proc. Combust. Inst. 33 (2011), pp. 1319–1330.

[11] V. Hiremath, S.R. Lantz, H. Wang, and S.B. Pope, *Large-scale parallel simulations of turbulent combustion using combined dimension reduction and tabulation of chemistry*, Proc. Combust. Inst. 34 (2013), pp. 205–215.

[12] Y. Yang, H. Wang, S.B. Pope, and J.H. Chen, *Large-eddy simulation/probability density function modeling of a non-premixed CO/H_2 temporally evolving jet flame*, Proc. Combust. Inst. 34 (2013), pp. 1241–1249.

[13] A. Gupta, D.C. Haworth, and M.F. Modest, *Turbulence–radiation interactions in large-eddy simulations of luminous and nonluminous nonpremixed flames*, Proc. Combust. Inst. 34 (2013), pp. 1281–1288.

[14] D.H. Rowinski and S.B. Pope, *An investigation of mixing in a three-stream turbulent jet*, Phys. Fluids 25 (2013), Paper No. 105105. Available at http://dx.doi.org/10.1063/1.4822434.

[15] T. Poinsot and D. Veynante, *Theoretical and Numerical Combustion*, 3rd ed., e-Learning@cerfacs, 2012.

[16] T.S. Kuan, R.P. Lindstedt, and E.M. Vaos, *Advances in Confined Detonations and Pulse Detonation Engines*, G.D. Roy, ed., Torus Press, Moscow, 2003.

[17] R.P. Lindstedt and E.M. Vaos, *Transported PDF modeling of high-Reynolds-number premixed turbulent flames*, Combust. Flame 145 (2006), pp. 495–511.

[18] M. Stöllinger and S. Heinz, *Evaluation of scalar mixing and time scale models in PDF simulations of a turbulent premixed flame*, Combust. Flame 157 (2010), pp. 1671–1685.

[19] B.T. Zoller, M.L. Hack, and P. Jenny, *A PDF combustion model for turbulent premixed flames*, Proc. Combust. Inst. 34 (2013), pp. 1421–1428.

[20] R. Borghi, *On the structure and morphology of turbulent premixed flames*, in *Recent Advances in the Aerospace Sciences*, C. Bruno and S. Casci, eds., Plenum Press, New York, 1985, pp. 117–138.

[21] H. Pitsch, *Large-eddy simulation of turbulent combustion*, Annu. Rev. Fluid Mech. 38 (2006), pp. 453–482.

[22] V. Hiremath, S. Lantz, H. Wang, and S.B. Pope, *Computationally-efficient and scalable parallel implementation of chemistry in simulations of turbulent combustion*, Combust. Flame 159 (2012), pp. 3096–3109.

[23] V. Hiremath, Z. Ren, and S.B. Pope, *Combined dimension reduction and tabulation strategy using ISAT-RCCE-GALI for the efficient implementation of combustion chemistry*, Combust. Flame 158 (2011), pp. 2113–2127.

[24] S.B. Pope, *Computationally efficient implementation of combustion chemistry using in situ adaptive tabulation*, Combust. Theory Model. 1 (1997), pp. 41–63.

[25] M. Bodenstein and S.C. Lind, *Geschwindigkeit der bildung des bromwasserstoffs aus seinen elementen*, Z. Phys. Chem. 57 (1906), pp. 168–175.

[26] M.D. Smooke (ed.), *Reduced Kinetic Mechanisms and Asymptotic Approximations for Methane–Air Flames*, Lecture Notes in Physics 384, Springer-Verlag, Berlin, 1991.

[27] Z. Ren, S.B. Pope, A. Vladimirsky, and J.M. Guckenheimer, *The invariant constrained equilibrium edge preimage curve method for the dimension reduction of chemical kinetics*, J. Chem. Phys. 124 (2006), Paper No. 114111. Available at http://dx.doi.org/10.1063/1.2177243.

[28] J.C. Keck and D. Gillespie, *Rate-controlled partial equilibrium method for treating reacting gas-mixtures*, Combust. Flame 17 (1971), pp. 237–241.

[29] J.C. Keck, *Rate-controlled constrained equilibrium theory of chemical reactions in complex systems*, Prog. Energy Combust. Sci. 16 (1990), pp. 125–154.

[30] S.B. Pope, *Gibbs function continuation for the stable computation of chemical equilibrium*, Combust. Flame 139 (2004), pp. 222–226.

[31] A. Sjunnesson, S. Olovsson, and B. Sjöblom, *Validation rig – a tool for flame studies*, in *Proceedings of the 10th International Symposium on Air Breathing Engines*, Nottingham, UK, 1–6 September 1991, Vol. 1, AIAA, Washington, DC, 1991, pp. 385–393.

[32] A. Sjunnesson, P. Henrikson, and C. Löfström, *CARS measurements and visualization of reacting flows in a bluff body stabilized flame*, in *Proceedings of the 28th Joint Propulsion Conference and Exhibit*, Nashville, TN, 6–8 July 1992, AIAA Paper No. 1992-3650.

[33] C. Fureby and S.I. Möller, *Large eddy simulation of reacting flows applied to bluff body stabilized flames*, AIAA J. 33 (1995), pp. 2339–2347.

[34] C. Fureby, *Large eddy simulation of combustion instabilities in a jet engine afterburner model*, Combust. Sci. Technol. 161 (2000), pp. 213–243.

[35] P. Nilsson and X.S. Bai, *Effects of flame stretch and wrinkling on co formation in turbulent premixed combustion*, Proc. Combust. Inst. 29 (2002), pp. 1873–1879.

[36] E. Giacomazzi, V. Battaglia, and C. Bruno, *The coupling of turbulence and chemistry in a premixed bluff-body flame as studied by LES*, Combust. Flame 138 (2004), pp. 320–335.

[37] P. Wang and X.S. Bai, *Large eddy simulation of turbulent premixed flames using level-set G-equation*, Proc. Combust. Inst. 30 (2005), pp. 583–591.

[38] C. Fureby, *Comparison of flamelet and finite rate chemistry LES for premixed turbulent combustion*, in *Proceedings of the 45th AIAA Aerospace Sciences Meeting and Exhibit*, Reno, NV, 8–1 January 2007, AIAA Paper No. 2007-1413.

[39] E. Baudoin, R. Yu, K.J. Nogenmyr, X.S. Bai, and C. Fureby, *Comparison of LES models applied to a bluff body stabilized flame*, in *Proceedings of the 47th AIAA Aerospace Sciences Meeting including The New Horizons Forum and Aerospace Exposition*, Orlando, FL, 5–8 January 2009, AIAA Paper No. 2009-1178.

[40] B. Manickam, J. Franke, S.P.R. Muppala, and F. Dinkelacker, *Large-eddy simulation of triangular-stabilized lean premixed turbulent flames: Quality and error assessment*, Flow Turbul. Combust. (2012), pp. 1–34.

[41] T. Ma, O.T. Stein, N. Chakraborty, and A.M. Kempf, *A posteriori testing of algebraic flame surface density models for LES*, Combust. Theory Model. 17 (2013), pp. 431–482.

[42] P.P. Popov, H. Wang, and S.B. Pope, *Specific volume coupling and convergence properties in hybrid particle/finite volume algorithms for turbulent reactive flows*, J. Comput. Phys., submitted for publication.

[43] S. Viswanathan, H. Wang, and S.B. Pope, *Numerical implementation of mixing and molecular transport in LES/PDF studies of turbulent reacting flows*, J. Comput. Phys. 230 (2011), pp. 6916–6957.

[44] O. Desjardins, G. Blanquart, G. Balarac, and H. Pitsch, *High order conservative finite difference scheme for variable density low Mach number turbulent flows*, J. Comput. Phys. 227 (2008), pp. 7125–7159.

[45] Y. Morinishi, T.S. Lund, O.V. Vasilyev, and P. Moin, *Fully conservative higher order finite difference schemes for incompressible flow*, J. Comput. Phys. 143 (1998), pp. 90–124.

[46] C.D. Pierce and P. Moin, *Progress-variable approach for large-eddy simulation of non-premixed turbulent combustion*, J. Fluid Mech. 504 (2004), pp. 73–97.

[47] M. Germano, U. Piomelli, P. Moin, and W.H. Cabot, *A dynamic subgrid-scale eddy viscosity model*, Phys. Fluids A: Fluid Dynam. 3 (1991), pp. 1760–1765.

[48] D.K. Lilly, *A proposed modification of the Germano subgrid-scale closure method*, Phys. Fluids A: Fluid Dynam. 4 (1992), pp. 633–635.

[49] S. Kang, G. Iaccarino, F. Ham, and P. Moin, *Prediction of wall-pressure fluctuation in turbulent flows with an immersed boundary method*, J. Comput. Phys. 228 (2009), pp. 6753–6772.

[50] R. McDermott and S.B. Pope, *A particle formulation for treating differential diffusion in filtered density function methods*, J. Comput. Phys. 226 (2007), pp. 947–993.

[51] H. Wang, P.P. Popov, and S.B. Pope, *Weak second-order splitting schemes for Lagrangian Monte Carlo particle methods for the composition PDF/FDF transport equations*, J. Comput. Phys. 229 (2010), pp. 1852–1878.

[52] H. Pitsch, *FlameMaster, a C++ computer program for 0D combustion and 1D laminar flame calculations*, Institut für Technische Mechanik, RWTH Aachen University, Aachen, Germany, 1998; software available at http://www.stanford.edu.bases-doc.univ-lorraine.fr/group/pitsch/CES.htm.

[53] M. Klein, A. Sadiki, and J. Janicka, *A digital filter based generation of inflow data for spatially developing direct numerical or large eddy simulations*, J. Comput. Phys. 186 (2003), pp. 652–665.

[54] A.M. Kempf, S. Wysocki, and M. Pettit, *An efficient, parallel low-storage implementation of Klein's turbulence generator for LES and DNS*, Comput. & Fluids 60 (2012), pp. 58–60.

[55] A.A. Konnov, *Detailed reaction mechanism for small hydrocarbons combustion: release 0.5*, 2000.

[56] P. Gokulakrishnan, R. Bikkani, M.S. Klassen, R.J. Roby, and B.V. Kiel, *Influence of turbulence–chemistry interaction in blow-out predictions of bluff-body stabilized flames*, in *Proceedings of the 47th AIAA Aerospace Sciences Meeting including The New Horizons Forum and Aerospace Exposition*, Orlando, FL, 5–8 January 2009, AIAA Paper No. 2009-1179.

[57] I.A. Dodoulas and S. Navarro-Martinez, *Large eddy simulation of premixed turbulent flames using the probability density function approach*, Flow Turbul. Combust. 90 (2013), pp. 645–678.

[58] V. Hiremath, Z. Ren, and S.B. Pope, *A greedy algorithm for species selection in dimension reduction of combustion chemistry*, Combust. Theory Model. 14 (2010), pp. 619–652.